C. R. Chimie 18 (2015) 1013–1029

Contents lists available at ScienceDirect

Comptes Rendus Chimie

www.sciencedirect.com

International Symposium on Air & Water Pollution Abatement Catalysis (AWPAC) – Catalytic pollution control for stationary and mobile sources

Synthesis of CuO/SBA-15 adsorbents for SO_x removal applications, using different impregnation methods

Synthèse d'adsorbants CuO/SBA-15 par différentes méthodes d'imprégnation, pour le piégeage des SO_x

Pierrick Gaudin [a], Sophie Dorge [b,*], Habiba Nouali [a], Joël Patarin [a], Jean-François Brilhac [b], Emmanuel Fiani [c], Matthieu Vierling [d], Michel Molière [e]

[a] *Équipe « Matériaux à porosité contrôlée», institut de science des matériaux de Mulhouse, UMR 7361 CNRS, université de Haute-Alsace, 3 bis, rue Alfred-Werner, 68093 Mulhouse cedex, France*
[b] *Laboratoire de gestion des risques et environnement, UHA, 3 bis, rue Alfred-Werner, 68093 Mulhouse cedex, France*
[c] *Service entreprises et éco-technologies, direction productions et énergies durables, ADEME – agence de l'environnement et de la maîtrise de l'énergie, 20, avenue du Grésillé, BP 90406, 49004 Angers cedex 01, France*
[d] *GE Energy, 20, avenue du Marechal-Juin, 90007 Belfort cedex, France*
[e] *IRTES – LERMPS, UTBM Sévenans, 90010 Belfort cedex, France*

ARTICLE INFO

Article history:
Received 17 November 2014
Accepted after revision 2 July 2015
Available online 8 September 2015

Keywords:
SBA-15 mesoporous material
Impregnation and ion exchange
Drying and calcination
Copper oxide (CuO)-based adsorbent
SO_x ($SO_2 + SO_3$) adsorption

Mots clés :
Matériaux mésoporeux SBA-15
Imprégnation et échange ionique
Séchage et calcination
Adsorbent à base d'oxyde de cuivre (CuO)
Adsorption de SO_x ($SO_2 + SO_3$)

ABSTRACT

In this paper, SBA-15 mesoporous silica based adsorbents were synthesized for the desulfurization of flue gas streams, by several methods (wet impregnation, incipient wetness impregnation and ion exchange). The influence of the drying and calcination conditions on the porous texture and the dispersion of the active phase (CuO), as well as the efficiency of the adsorbents for SO_x trapping, were studied. Depending on the synthesis conditions, copper species are present as large CuO particles (1 μm) and/or as homogeneously dispersed species, undetectable by XRD/TEM. The SO_x adsorption efficiency seems to be closely related to the undetected copper species.

RÉSUMÉ

Différents adsorbants ont été synthétisés à partir de silice mésoporeuse SBA-15 pour la désulfuration d'effluents gazeux. Trois méthodes d'imprégnation (voie humide, à sec et échange ionique) ont été testées. L'influence des conditions de séchage et de calcination sur la texture poreuse, la dispersion de la phase active (CuO), ainsi que l'efficacité des matériaux pour la chimisorption des SO_x ont été étudiées. En fonction des conditions de synthèse, le cuivre est présent sous forme de grosses (1 μm) particules de CuO et/ou d'espèces uniformément dispersées et non détectées par DRX/MET. L'efficacité des adsorbants semble étroitement liée aux espèces cuivriques non détectées.

* Corresponding author.
E-mail addresses: pierrick.gaudin@uha.fr (P. Gaudin), sophie.dorge@uha.fr (S. Dorge), habiba.nouali@uha.fr (H. Nouali), joel.patarin@uha.fr (J. Patarin), jean-francois.brilhac@uha.fr (J.-F. Brilhac), emmanuel.fiani@ademe.fr (E. Fiani), matthieu.vierling@ge.com (M. Vierling), michel.moliere@utbm.fr (M. Molière).

http://dx.doi.org/10.1016/j.crci.2015.07.002
1631-0748/

1. Introduction

Gaseous SO_x emissions mainly originate from fossil fuel-fired combustion plants used for electricity and/or heat production, for instance gas turbines burning liquid fossil fuels. Besides their corrosive effect, SO_x are harmful to human health and the environment since they are a primary cause of acid rain [1] and a major precursor of secondary aerosols in the atmosphere. The long-standing concern regarding air pollution has led to more stringent SO_x emissions regulations, which have been made possible thanks to the development and the implementation of various flue gas desulfurization (FGD) processes. Nowadays, wet and dry scrubbing [2] are the main technologies implemented in industrial processes and in combustion plants. Wet scrubbing consists in spraying an aqueous solution of alkali or alkali earth metal base (NaOH; $Ca(OH)_2$, etc.) in the flue gas stream, which reacts with SO_x to form the corresponding sulfates, while the dry process is mainly performed by injecting a dry alkali earth salt such as $CaCO_3$. Despite their proven performance in terms of SO_x removal, these technologies suffer from several disadvantages, including significant energy consumption, the use of large amounts of reagents, the production of large amounts of wastes ($CaSO_4$, Na_2SO_4) and their non-regenerability.

Dry regenerative processes consisting in adsorbing SO_x on metal oxides are being investigated as an alternative to wet and dry scrubbing technologies. Such processes are based on bifunctional materials that first oxidize SO_2 to SO_3 (Eq. (1)) then chemisorb SO_3 as metal sulfate (Eq. (2)). Moreover, to make the process economically and environmentally sustainable, these adsorbents must be regenerable without any significant loss in SO_x trapping performances along multiple adsorption-regeneration cycles. The regeneration of the sulfated adsorbent is usually performed by thermal decomposition of the metal sulfate (Eq. (3)).

$$SO_2 + {}^1/_2O_2 \rightarrow SO_3 \quad (1)$$

$$xSO_3 + MO_x \rightarrow M(SO_4)_x \quad (2)$$

$$M(SO_4)_x \rightarrow xSO_3 + MO_x \quad (3)$$

Over the past decades, numerous studies dealing with SO_x chemisorption using dry regenerative processes were reported in the literature [2]. As reviewed by Mathieu et al., numerous materials were tested as adsorbents including single oxides (CaO, MgO, TiO_2, MnO_2, CeO_2, Al_2O_3), supported oxides on carbonaceous materials or on alumina, zeolites, clays, as well as mixed oxides, etc. [2]. Among all these material candidates, supported copper oxide has emerged as a good performer since it boasts:

- a high catalytic activity for the oxidation of SO_2 to SO_3;
- good SO_3 chemisorption as $CuSO_4$ [3–6];
- is regenerable at a moderate temperature (600 °C) that keeps intact its textural and morphological properties and limits the energy consumption.

Nevertheless, as already observed in previous studies [3], sulfation of copper oxide is affected by diffusion effects and is mainly limited to superficial copper atoms. Thus, in view of maximizing the sulfation degree, optimizing the dispersion of copper oxide has become "the heart of the matter". In this context, the strategy followed in the present study has consisted in dispersing copper oxide on a silica-based mesoporous support likely to ensure a high dispersion of the active phase thanks to its high surface area. Indeed, since their discovery, mesoporous silica materials have been widely employed as hosts for different metal oxides including copper oxide [7–15]. Several considerations led to select SBA-15 as support in this work. Firstly, silica is inert towards SO_x which prevents the support from sulfating and the mesoporous structure from collapsing. Secondly, SBA-15 enjoys very high porous volume and surface area properties. Additionally, its pore size lies in the range of 5–10 nm and thus enables the transport of reactants such as SO_x in the mesoporous channels. It has been reported that the dispersion of the active phase depends on the impregnation method [16–19], the metal precursor [19,20], the support [17,19] and the solvent used [21], as well as the drying [18,22] and calcination conditions [17,23–32]. Previous works dealing with the synthesis of supported metals or metal oxides on mesoporous silica have indicated that the growth of metal oxide particles during calcination may lead to pore plugging [16,26,29,33] and/or the migration of metal oxide outside the porous structure [16,29,31]. In this study, the dispersion of CuO on SBA-15 was investigated through different impregnation methods consisting in:

- wet impregnation;
- incipient wetness impregnation;
- ion exchange.

This latter method is not really an impregnation method but rather a deposit method for addition of active phase. However in the following of the text, this spelling will be kept. The choice of these impregnation methods was done to be compatible with a potential industrial application. The influence of the solvent, as well as the drying and calcination conditions was also studied. The resulting adsorbents were characterized by nitrogen physisorption, X-Ray Diffraction (XRD), X-ray Fluorescence (XRF), Scanning (SEM) and Transmission Electron Microscopy (TEM). The SO_x storage capacity of the adsorbents was determined using a fixed bed reactor using a Gas Hourly Space Velocity (GHSV) as high as 25,000 h^{-1}, to be representative of gas turbine applications that are characterized by high flue gas flow rates.

2. Experimental part

2.1. Synthesis of SBA-15

The SBA-15 mesoporous silica was synthesized as follows: 210 g of pluronic 123 (Sigma-Aldrich) were dissolved in a solution containing 1000 mL of HCl (37%, Sigma-Aldrich) and 6600 mL of distilled water, at 55 °C in a 10 L container. After complete dissolution, 450 g of tetraethylorthosilicate (Sigma-Aldrich) were added and

the solution was kept under stirring for 24 h at 55 °C. The temperature was then increased until 90 °C for 24 h. The precipitate obtained was filtered, washed with distilled water, dried at 90 °C overnight and calcined at 300 °C for 6 h (ramp of 1 °C·min^{-1}) in order to remove the organic template.

2.2. Preparation of the CuO/SBA-15 adsorbents

Three impregnation methods consisting in Wet Impregnation (WI), Incipient Wetness Impregnation (IWI) and Ion Exchange (IE) were investigated. For the WI method, two solvents (water or methanol) were used. Methanol has been used as a solvent since its polar character allows a good solubility of copper nitrate and its low boiling point (65 °C) makes its evaporation fast and easy at ambient pressure. For each impregnation method, several drying and calcination conditions were evaluated. The drying step lasted 24 h and was performed:

- at room temperature;
- in an oven at 45 °C or 90 °C or;
- by lyophilization.

Two calcination (in muffle furnace) conditions were used: the "ramp calcination" consisted in heating the sample at 500 °C for 6 h after a ramp of 1 °C·min^{-1}; the "flash calcination" consisted in introducing and keeping for 6 h the sample in a furnace preheated at 500 °C.

2.2.1. Preparation of CuO/SBA-15 by Wet Impregnation in methanol (WIm) or water (WIw)

The impregnation was performed by dissolving 622 mg of $Cu(NO_3)_2.3H_2O$ (Sigma-Aldrich) in a beaker containing 60 mL of (i) methanol (Sigma-Aldrich) or (ii) water. 1.0 g of calcined SBA-15 was added to this solution and the mixture was stirred at room temperature for 2 h. The methanol-based solution was then introduced in a bath at 60 °C under stirring until the methanol was completely evaporated. The water based solution was evaporated in 2 h using a rotary evaporator at 30 °C under reduced pressure (20 mbar). Both resulting powders were dried and calcined to obtain copper oxide.

2.2.2. Preparation of CuO/SBA-15 by Incipient Wetness Impregnation in water (IWIw)

The general IWI consists in impregnating the porous material with a volume of a precursor-laden solution which corresponds exactly to its porous volume previously determined by N_2 physisorption. This general procedure was slightly modified, the volume of the solution being twice the one of the porous volume of the SBA-15 in order to impregnate both internal and external surfaces. Thus, 610 mg of $Cu(NO_3)_2.3H_2O$ were dissolved in 2.4 mL of distillated water and put in contact with 1.0 g of calcined SBA-15 (porous volume of 1.2 g·cm^{-3}). The resulting powder was dried and calcined yielding the CuO/SBA-15 adsorbent.

2.2.3. Preparation of CuO/SBA-15 by Ion Exchange (IE)

The adsorbents obtained by IE were prepared as follows: 800 mg of $Cu(NO_3)_2.3H_2O$ were dissolved in 25 mL of distillated water and the pH was adjusted to 10.5 by adding a 30 wt. % of ammonia solution. The solution was then cooled at 0 °C in an ice/water bath in order to limit the hydrolysis of silica. Then 1.0 g of calcined SBA-15 was added to the solution and the mixture was kept for 30 min at 0 °C under stirring. The solid was then recovered by filtration, washed two times for 30 min in 30 mL of distillated water, dried and calcined.

2.3. Samples nomenclature

In this work, samples are named according to: (i) their Impregnation Method (IM), (ii) the solvent used (s), (iii) the drying conditions (dc) and (iv) the calcination procedure (cp), resulting in the following notation: "IMs-dc-cp". In the case of wet impregnation, the samples impregnated with methanol are designated by the prefix "WIm" and those impregnated with water by "WIw". The samples designation further includes an infix which is: "no" for undried samples; "20", "45", "90" and "lyo" for the samples dried at 20 °C, 45 °C, 90 °C and by lyophilization, respectively. The two calcination procedures are distinguished by a suffix which is "r" (ramp calcination) or "f" (flash calcination). As an example, the sample obtained by wet impregnation in methanol, dried at 45 °C and calcined with a ramp is named "WIm-45-r".

2.4. Characterization techniques

X-Ray powder Diffraction (XRD) patterns were obtained in the reflection mode with a PANalytical X'Pert diffractometer (Cu Kα radiation, λ = 1.5418 Å) equipped with a X'Celerator detector. Measurements were achieved for 2θ angles in the 3–70° range, by step of 0.02° (220 s by step). The same diffractometer was used to record the XRD patterns at low angles (2θ range: 0.5–3°). In that case, a glass support was used as sample holder. Transmission Electron Microscopy (TEM) micrographs were taken with a Philips CM200 microscope equipped with a LaB_6 filament. The accelerating voltage was 200 kV. Samples were previously dispersed in water and sonicated during 10 min. Then five to ten drops of the solution were deposited onto Cu grids coated with a thin (5 nm thickness) holey carbon support film. Copper analyses were performed using a X-Ray Fluorescence (XRF) spectrometer (Philips MagiX) on samples compacted in 13 mm diameter pellets. Nitrogen physisorption were carried out on a Micromeritics Tristar apparatus. Prior to the measurements, the samples were outgassed at 150 °C for 15 h under primary vacuum. Specific surface areas and pore size distributions were determined by the BET and BJH methods respectively. Scanning Electron Microscopy (SEM) micrographs were obtained with a Philips XL 30 FEG microscope. Cu X-ray mappings were obtained from the EDX analyzer Oxford Inca Si(Li) integrated in the same microscope.

2.5. SO_2 adsorption tests

The SO_2 adsorption tests were performed in a fixed bed reactor. The CuO/SBA adsorbents were previously pelletized (2 min at 0.25 ton·cm^{-2}), crushed and sieved to retain

the 225–450 μm portion. Samples were introduced in a vertical quartz reactor (6 mm inner diameter) fitted with a fused silica layer. The adsorption experiments were performed at 400 °C using a gas mixture containing 250 ppm of SO_2 and 10 vol. % of O_2 in nitrogen. The gas flow rate equalling 13 $NL{\cdot}h^{-1}$, was adjusted by BROOKS 5850 mass flow controllers. The height of the adsorbent bed in the reactor was set at 2 cm in order to reach the high GHSV value of 25,000 h^{-1} which is representative of gas turbine exhaust conditions. The SO_2 outlet concentration was continuously measured by an UV absorption analyzer (Rosemount NGA 2000; range: 0–1000 ppm). The accuracy of the measurements, given by the manufacturer, is better than 1% of full scale. Before the SO_2 adsorption phase, the adsorbent was heated from 25 to 400 °C at a 5 $°C{\cdot}min^{-1}$ rate under pure N_2 and the temperature was maintained at 400 °C during 1 h. The dynamic SO_2 adsorption capacity (C_{ads}) expressed in mg of SO_2 per gram of adsorbent (adsorbent = active phase + - support SBA-15) ($mg_{SO_2}{\cdot}g_{adsorbent}{}^{-1}$) was calculated by integration of the SO_2 breakthrough curve until the SO_2 concentration reaches the 75 ppm (vol.) threshold value at the outlet of the reactor. This value has been chosen in order to match the SO_x emission limit enacted by the European legislation. The calculation is performed as follows:

$$\frac{Q_g \times M_{SO_2}}{10^3 \times V_m} \times \frac{\int_{t_0}^{t_{75}} (C_0 - C)\mathrm{d}t}{m_{ads}}$$

where Q_g is the gas flow rate ($NL{\cdot}s^{-1}$), V_m is the molar volume (equaling 22.4 L at 0 °C and 1 atmosphere), M_{SO_2} the molar mass of SO_2 ($g{\cdot}mol^{-1}$), C_0 and C are respectively the inlet (250 ppm) and outlet concentrations of SO_2 (in ppm), m_{ads} is the mass of the adsorbent (gram) and t_o and t_{75} (s) are respectively the starting time and the time at which the SO_2 concentration reaches 75 ppm.

3. Results

3.1. Wet Impregnation in methanol (WIm)

The chemical composition, color, textural properties and SO_2 uptake capacities of the adsorbents obtained by Wet Impregnation in methanol (WIm) are given in Table 1. Methanol has been used as a solvent since its polar character allows a good solubility of copper nitrate and its low boiling point (65 °C) makes its evaporation fast and easy at ambient pressure.

All samples have a copper oxide loading around 17–18 wt. %. Five distinct drying conditions (no drying, drying at 20 °C, 45 °C, 90 °C and lyophilization) and two calcination conditions (ramp and flash) are compared.

It can be observed that the color of the obtained adsorbents is closely related to the drying and calcination conditions. It is noteworthy that samples WIm-no-f, WIm-45-f, WIm-90-r and WIm-lyo-r are heterogeneous as they present some green and blue areas in the crucible after calcination. This suggests that different copper species are formed during the impregnation, drying and calcination steps. Indeed, XRD analysis (not reported here) of the blue particles reveals the presence of crystalline CuO phase (PDF4+ 00-005-0661) while for the green ones, no peaks are observed suggesting either the formation of a very thin CuO film as reported by Tian et al. [34] or the presence of copper species in strong interaction with the support, e.g., Cu–O–Si species [25,35]. Since all SBA-15 samples were impregnated under stirring and further homogenized by crushing before the drying and calcination steps, this heterogeneity must come from the drying and/or calcination steps. After a number of tests of drying and calcination, we observed that when the powder is laid as a fine, homogeneous layered in the calcination vessel, the resulting adsorbent is generally homogenous. In contrast, when the impregnated material is laid as a thick layer, heterogeneous samples are preferentially formed. A similar phenomenon was observed by Sun et al. [32] who reported the strong effect of that they called "container effect" by comparing the adsorbents obtained by calcination of mesoporous silica (KIT-6) impregnated with metal nitrate precursor, in closed or open reactors. They observed that in a closed reactor, the formation of large metal oxide particles was favored. This effect was attributed to the slow escape rate of the hydration water vapor and decomposition gases (NO, NO_2, O_2) of the nitrate precursor. Indeed, these gases (H_2O, NO, NO_2, O_2) were reported to significantly increase the size of the metal oxide particles by accelerating their sintering [23,24,26,29,32]. Except for the lyophilized samples, the flash calcination tends to lead to the formation of heterogeneous materials (with and without drying at 45 °C: WIm-no-f and WIm-45-f, respectively). On the contrary the calcination with a ramp seems to favor homogenous materials (WIm-no-r, WIm-20-r, WIm-45-r),

Table 1
Synthesis conditions, textural properties, chemical composition and SO_2 uptake capacities of the adsorbents prepared by Wet Impregnation in methanol (WIm).

Sample	SBA-15	WIm-no-r	WIm-no-f	WIm-20-r	WIm-45-r	WIm-45-f	WIm-90-r	WIm-lyo-r	WIm-lyo-f
Drying (24 h)	–	No	No	20 °C	45 °C	45 °C	90 °C	Lyoph.	Lyoph.
Calcination	Ramp	Ramp	Flash	Ramp	Ramp	Flash	Ramp	Ramp	Flash
Color	White	Green-grey	Green + blue	Green	Green	Green + blue	Dark blue + green	Green + blue	Green
CuO content (wt. %)	0	–	–	17.4	18.2	17.9	–	–	–
S_{BET} ($m^2{\cdot}g^{-1}$)	938	591	625	554	553	591	556	576	637
V_p ($cm^3{\cdot}g^{-1}$)	1.2	0.8	0.8	0.7	0.7	0.8	0.7	0.8	0.8
Pore size (nm)	7.5	7.6	7.7	7.7	7.5	7.6	7.5	7.6	7.7
SO_2 uptake ($mg_{SO_2}{\cdot}g_{ads}{}^{-1}$)	/	15	27	9	12	30	2	15	27

except for the adsorbents dried by lyophilization (WIm-lyo-r) and at 90 °C (WIm-90-r). For the latter, the predominant dark blue color suggests the formation of substantial amount of large CuO particles as confirmed by the corresponding XRD pattern that show the most intense CuO peaks (Fig. 1). Indeed, it was reported that the drying at "high temperature" (~ 100 °C) favors the formation of large CuO crystallites compared to the drying at 25 °C [18,25]. This effect might be assigned to the formation of nitrate hydroxide ($Cu_2(OH)_3(NO_3)$) which tends to concentrate in the wet spots that remain during the last vaporization stages, resulting in large CuO particles after calcination. In contrast, for the sample dried at 25 °C, a green color and no diffraction peaks are observed [18].

It can be noticed that although the copper loading is in the same order of magnitude for all samples, there are strong differences in the peak intensity. Moreover, similarly to the results of Munnik et al. [25], peak broadening is observed for none of samples. This result suggests a bimodal distribution of the copper species which seems to form either large crystalline CuO particles (detected by XRD) or XRD-undetected copper species. As discussed below, the SEM micrographs and X-ray mappings suggest that the undetected copper species are very homogeneously dispersed on the mesoporous support. The samples dried in different conditions and calcined with a ramp show the smaller XRD peak intensities with the ranking: WIm-no-r < WIm-45-r < WIm-lyo-r < WIm-20-r. The sample WIm-lyo-f shows comparably low peak intensities although it was obtained by flash calcination. The other adsorbents obtained by flash calcination (WIm-no-f and WIm-45-f) show intense CuO peaks. As discussed above, the highest intensity is observed for the sample WIm-90-r which has been dried at 90 °C. In summary, as a general trend, the combination of a calcination step with a ramp and a low drying temperature step (especially the drying by lyophilization) seems to favor the formation of undetected copper species rather than large CuO particles.

The nitrogen physisorption isotherms of the SBA-15 adsorbent and those of representative sorbents obtained for each impregnation method (WIm, WIw, IWIw, and IEw) are reported in the Fig. 2. The isotherms of the SBA-15 shows parallel adsorption and desorption branches and a well-defined hysteresis loop in the relative pressure range $p/p^0 = 0.7–0.8$. It corresponds to the type IV according to the IUPAC classification and is characteristic of mesoporous material with well-ordered cylindrical pores [36]. As it will be discussed below, the shape of the adsorption-desorption branches of the adsorbents differs in function of the impregnation method. However, given an impregnation method, whatever the drying or calcination treatment, the samples display similar isotherms (for the sake of concision, this result is not illustrated by a figure). The N_2 isotherms corresponding to the adsorbent WIm-lyo-r reported in Fig. 2 suggest that the mesoporous structure of SBA-15 is not altered by the WIm method. The pore volumes and specific surface areas are indicated in Table 1. As expected, the pore volumes of the CuO/SBA-15 adsorbents (0.7 to 0.8 $cm^3 \cdot g^{-1}$) are smaller than that of the SBA-15 calcined at 500 °C (1.2 $cm^3 \cdot g^{-1}$); this is mainly attributed to the densification of the mesoporous support due to the incorporation of copper oxide. A partial pore plugging of the mesoporous support by CuO particles is also possible and also could explain this pore shrinkage effect. The same trend is observed for the specific surface areas that range from 553 to 637 $m^2 \cdot g^{-1}$ for the CuO/SBA-15 versus 938 $m^2 \cdot g^{-1}$ for unloaded SBA-15. However, the incorporation of copper does not influence significantly the pore size distribution (determined by applying the BJH method on the desorption branch) which is centered between 7.5 and 7.7 nm for all samples, including the non-impregnated adsorbent. When comparing the CuO/SBA-15 adsorbents, it is noteworthy that the flash-calcined samples exhibit slightly higher specific BET surface areas (590 to 640 $m^2 \cdot g^{-1}$) as compared to those calcined with a ramp (553 to 591 $m^2 \cdot g^{-1}$). In contrast, the preparation

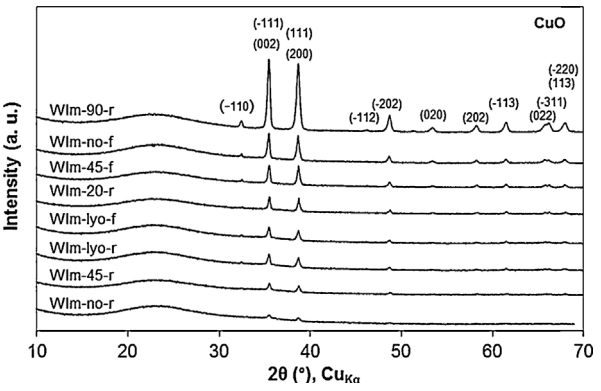

Fig. 1. XRD patterns of CuO/SBA-15 adsorbents prepared by Wet Impregnation in methanol (WIm). For a better visibility, the diffraction patterns are shifted along the *Y*-axis.

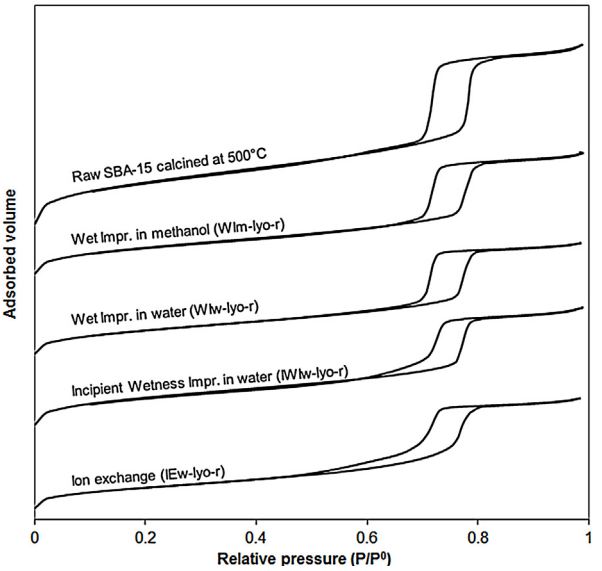

Fig. 2. Nitrogen adsorption-desorption isotherms of raw SBA-15 and CuO/SBA-15 adsorbents obtained by: Wet Impregnation in methanol (WIm-lyo-r) or in water (WIw-lyo-r); Incipient Wetness Impregnation in water (IWIw-lyo-r) and Ion Exchange in water (IEw-lyo-r). For a better visibility, the isotherms are shifted along the *Y*-axis.

method does not significantly impact on the pore volume which ranges between 0.7 and 0.8 $cm^3 \cdot g^{-1}$ for all samples.

The SEM micrographs and the corresponding X-ray mappings of samples WIm-90-r, WIm-no-r and WIm-no-f are shown in Fig. 3. As expected from the XRD pattern (Fig. 1), the X-ray mapping (EDX) of WIm-90-r (Fig. 3B) shows copper mainly distributed in large CuO particles that are also visible on the corresponding micrograph (Fig. 3A). On the contrary, no large CuO particles are detected for the sample WIm-no-r (Fig. 3C) and the corresponding X-ray mapping (Fig. 3D) shows instead a homogeneous distribution of copper species on the support. This result fits well with the XRD patterns that exhibit very weak CuO peaks for this adsorbent (Fig. 1). The X-ray mapping (Fig. 3F) of the adsorbent WIm-no-f shows large CuO particles similar to those of WIm-90-r but a greater fraction of copper remains homogeneously dispersed on the support. This is also in agreement with the corresponding XRD patterns of Fig. 1.

The TEM micrographs of samples WIm-90-r, WIm-no-r, WIm-no-f, WIm-lyo-r, WIm-lyo-f are reported in Fig. 4. In accordance with the XRD, SEM and X-ray mapping analyses, large CuO crystallites ($\sim$ 2 μm), are evidenced for the sample WIm-90-r (Fig. 4A). These particles are found outside the pores while the porous structure of the SBA-15 support is fairly conserved after the impregnation, drying and calcination steps (Fig. 4B). This is in accordance with the adsorption-desorption isotherms (Fig. 2). The micrographs C–J (Fig. 4) of the other samples confirm the conservation of the porous structure of the support but do not reveal the presence of copper particles, suggesting the formation of either a thin, homogeneously dispersed CuO film or superficial Cu–O–Si species, as discussed above.

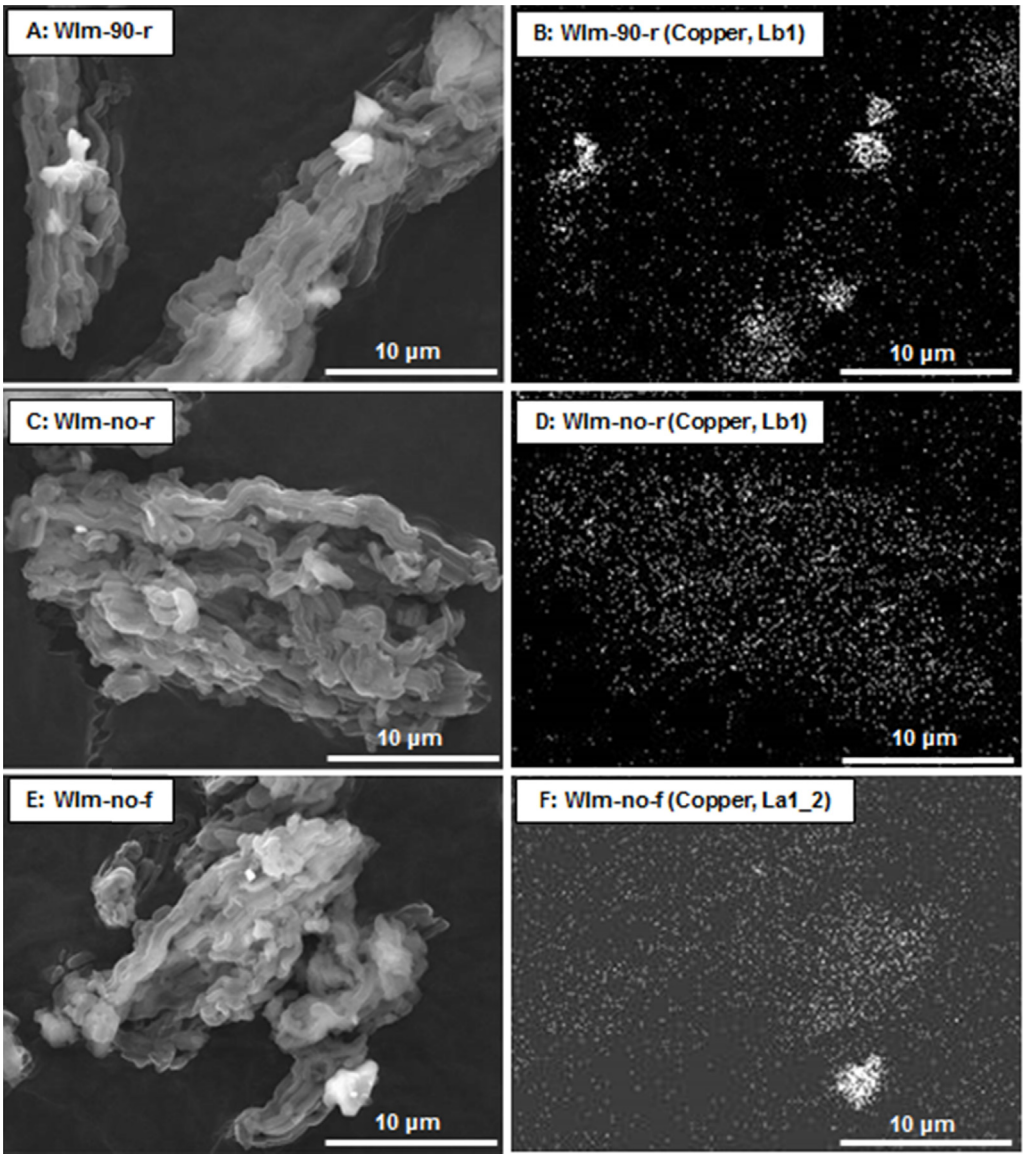

Fig. 3. SEM micrographs (A, C and E) and corresponding X-ray mappings of copper (B, D and F) of samples WIm-90-r, WIm-no-r and WIm-no-f, respectively.

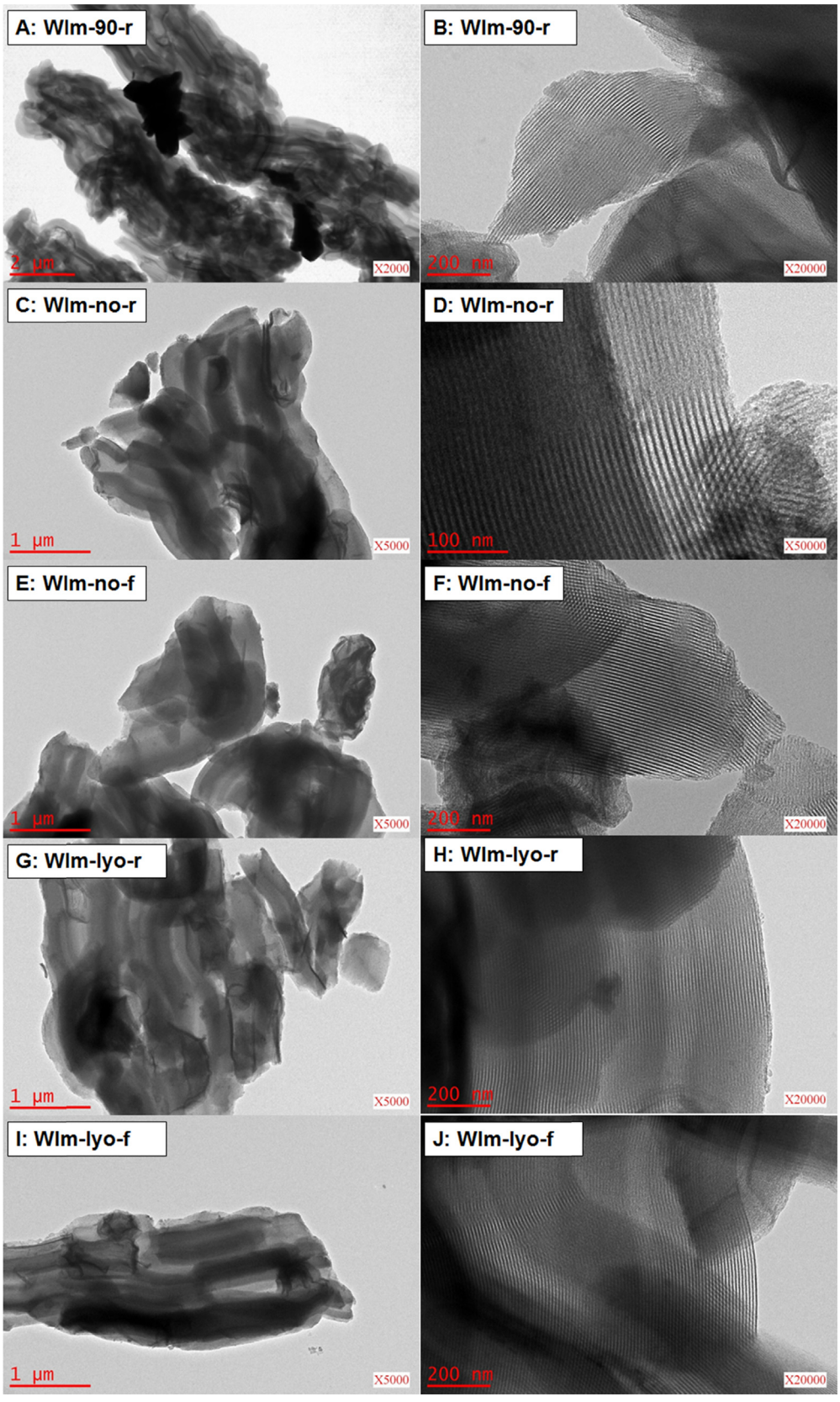

Fig. 4. (Color online.) TEM micrographs of samples WIm-90-r (A and B), WIm-no-r (C and D), WIm-no-f (E and F), WIm-lyo-r (G and H) and WIm-lyo-f (I and J), obtained by Wet Impregnation in methanol (WIm).

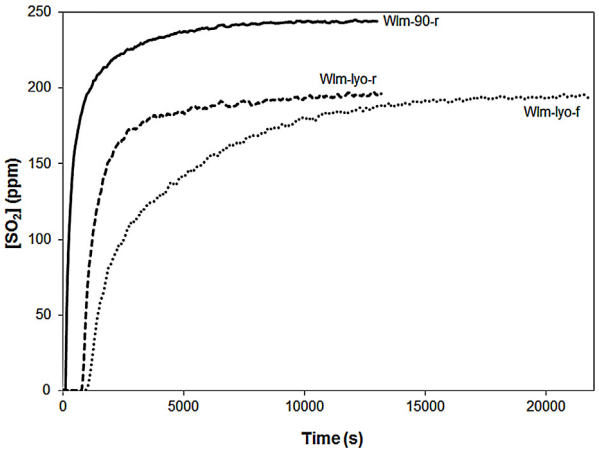

Fig. 5. SO_2 Breakthrough curves of samples WIm-90-r, WIm-lyo-r and WIm-lyo-f.

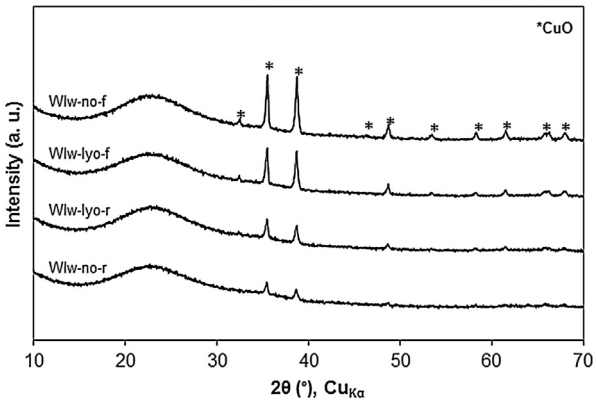

Fig. 6. XRD patterns of CuO/SBA-15 samples prepared by Wet Impregnation in water (WIw). For a better visibility, the diffraction patterns are shifted along the *Y*-axis.

The SO_2 adsorption performances of the adsorbents impregnated by WI using methanol were evaluated. The SO_2 breakthrough curves of samples WIm-90-r, WIm-lyo-r and WIm-lyo-f are shown for example in Fig. 5, the SO_2 uptake capacities of all adsorbents being summarized in Table 1.

The SO_x saturation of the WIm-90-r sample occurs very quickly meaning a small SO_2 adsorption capacity (2 $mg_{SO_2} \cdot g_{ads}^{-1}$), which can be attributed reasonably to the formation of large CuO particles as shown above. Indeed Centi et al. have observed that sulfation of pure CuO occurs very slowly and they assumed that there is a rapid formation of superficial sulfate species, which, because of the higher cell volume of $CuSO_4$ compared to that of CuO, slow down the formation of subsurface sulfate species [3]. The adsorbents WIm-lyo-r and WIm-lyo-f exhibit a significantly higher SO_2 uptake capacity with SO_2 adsorption curves showing similar breakthroughs, at around 800 s, but different shapes. Indeed, the SO_2 saturation profile of the WIm-lyo-r adsorbent is sharper than that of the WIm-lyo-f, suggesting that the chemisorption of SO_2 in the latter suffers from kinetic limitations. At $[SO_2]_{out}$ = 75 ppm, the measured SO_2 uptake capacity of WIm-lyo-f is higher than that of WIm-lyo-r (27 $mg_{SO_2} \cdot g_{ads}^{-1}$ versus 15 $mg_{SO_2} \cdot g_{ads}^{-1}$). Fig. 5 shows that, at the saturation of the three adsorbents, the SO_2 concentration at the outlet of the reactor is around 200–240 ppm of SO_2 whereas the concentration of injected SO_2 is 250 ppm. This means that a fraction of the injected SO_2 is still oxidized by the adsorbent, yielding SO_3 which is not detected by the UV analyzer.

From Table 1, it appears that the adsorbents that underwent a flash calcination, WIm-no-f, WIm-45-f and WIm-lyo-f are surprisingly the most efficient ones, with SO_2 uptake capacities of 27, 30 and 27 $mg_{SO_2} \cdot g_{ads}^{-1}$, respectively, although they show fairly high XRD peaks of copper oxide (Fig. 1). The adsorbents calcined with a ramp of temperature exhibit the lower SO_2 chemisorption capacities. Therefore, it is rather difficult to correlate the SO_2 uptake capacities with the XRD patterns. In summary, the overall set of investigations suggests that copper exhibits a bimodal distribution consisting on one hand in large CuO particles and on the other hand, in homogeneously dispersed XRD-undetected copper species. The predominance of one kind of species over the other seems to be closely related to the drying and calcination steps. According to the work of Centi et al. and in agreement with results obtained in this work for sample WIm-90-r, it seems reasonable to assume that large crystalline CuO particles are poorly active in the $DeSO_x$ reaction and the efficiency of the adsorbent is mainly due to the undetected copper species. According to the SO_2 uptake capacity data reported in Table 1, it seems that the flash calcination enhances the formation of efficient copper species for the $DeSO_x$ reaction.

3.2. Wet Impregnation in water (WIw)

In order to evaluate the influence of the solvent, the same batch of SBA-15 was impregnated following the same

Table 2
Synthesis conditions, textural properties, chemical composition and SO_2 uptake capacities of the adsorbents prepared by Wet Impregnation in water (WIw).

Sample	WIw-no-r	WIw-no-f	WIw-lyo-r	WIw-lyo-f
Drying (24 h)	No	No	Lyoph.	Lyoph.
Calcination	Ramp	Flash	Ramp	Flash
Color	Grey-green	Green + blue	Green	Green + blue
CuO content (wt. %)	18.0	18.2	18.3	17.7
S_{BET} ($m^2 \cdot g^{-1}$)	509	485	502	520
V_p ($cm^3 \cdot g^{-1}$)	0.7	0.7	0.7	0.7
Pore size (nm)	7.6	7.6	7.5	7.6
SO_2 uptake ($mg_{SO_2} \cdot g_{ads}^{-1}$)	49	27	13	18

protocol but using water instead of methanol according to the WIw protocol. The characterization of the resulting adsorbents is summarized in Table 2 that aims at comparing two distinct drying methods (no drying and lyophilization) and two calcination methods (ramp and flash).

The four samples have a copper loading close to 18 wt. %. Observations similar to the case of impregnation with methanol can be made in terms of sample heterogeneity, XRD patterns (Fig. 6) and inferable CuO dispersion status.

Here also, the shape of the N_2 physisorption isotherms of the adsorbent WIw-lyo-r (Fig. 2) is similar to that of the original SBA-15, suggesting the absence of alterations caused by the solvent on the mesoporous structure. The pore size distributions (7.5–7.6 nm) and pore volumes (0.7 $cm^3 \cdot g^{-1}$) reported in Table 2 are close to those reported for the WIm samples but the specific surface areas of the WIw samples are this time much less dependent from the synthesis procedure. The SEM micrographs of samples WIw-no-r, WIw-no-f and WIw-lyo-r and their corresponding X-ray mappings are reported in Fig. 7. For the adsorbents calcined with a ramp, i.e. WIw-no-r (Fig. 7 A and B) and WIw-lyo-r (Fig. 7 E and F), the copper seems to be mainly homogeneously distributed with no detected large CuO particles, which is in good agreement with the weak intensity of the CuO peaks of the corresponding XRD patterns (Fig. 6). On the contrary, the WIw-no-f adsorbent (Fig. 7C and D) exhibits a fraction of copper that is homogeneously dispersed on the support; one sees also large ($\sim$ 1 μm) CuO particles, as expected from the intense signal observed on the XRD pattern.

TEM micrographs of WIw-no-r (A and B), WIw-no-f (C and D) and WIw-lyo-r (E and F) are shown in Fig. 8. They do not reveal CuO particles in the porous structure. In

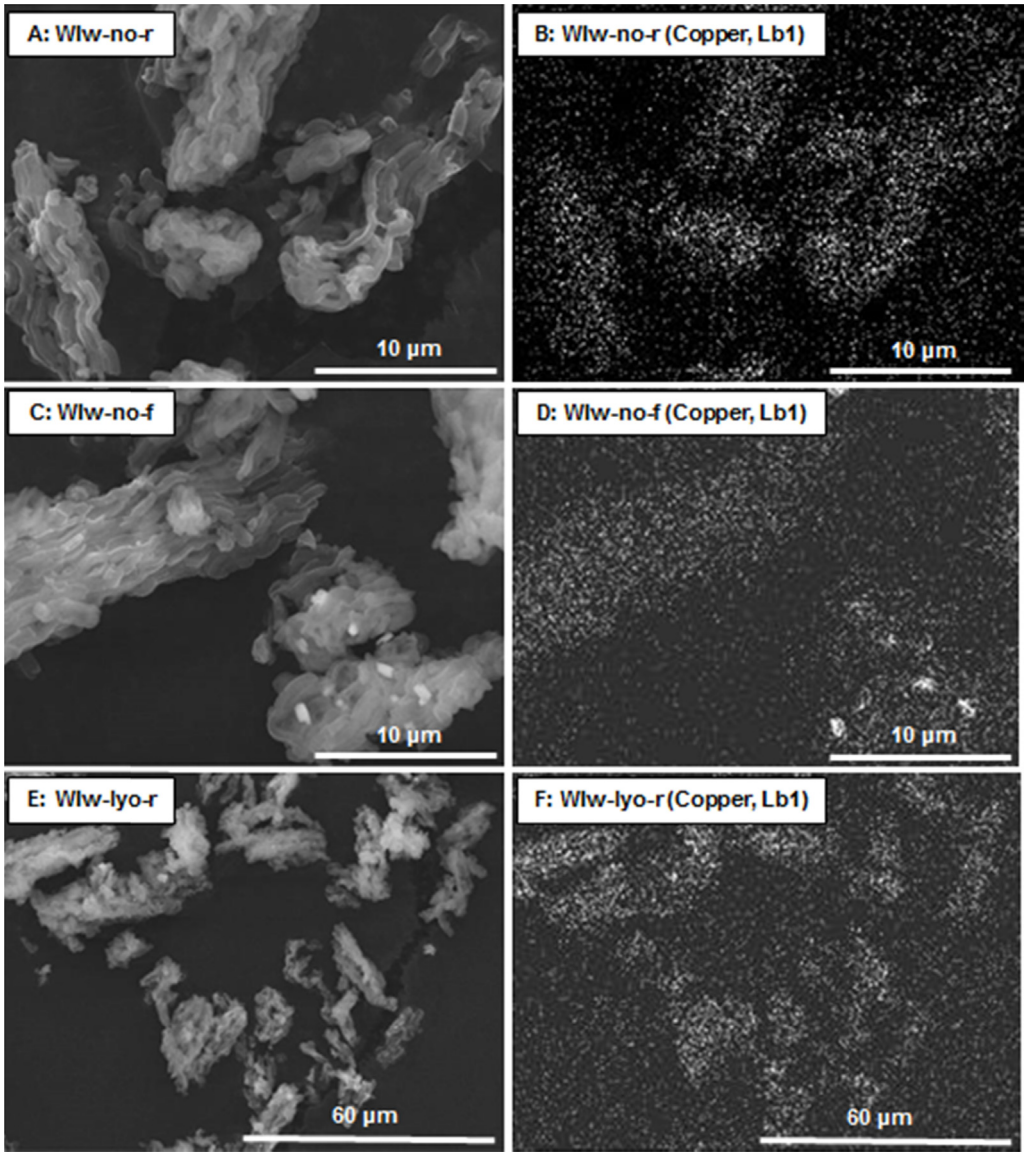

Fig. 7. SEM micrographs (A, C and E) and corresponding X-ray mappings (B, D and F) of samples WIw-no-r, WIw-no-f and WIw-lyo-r.

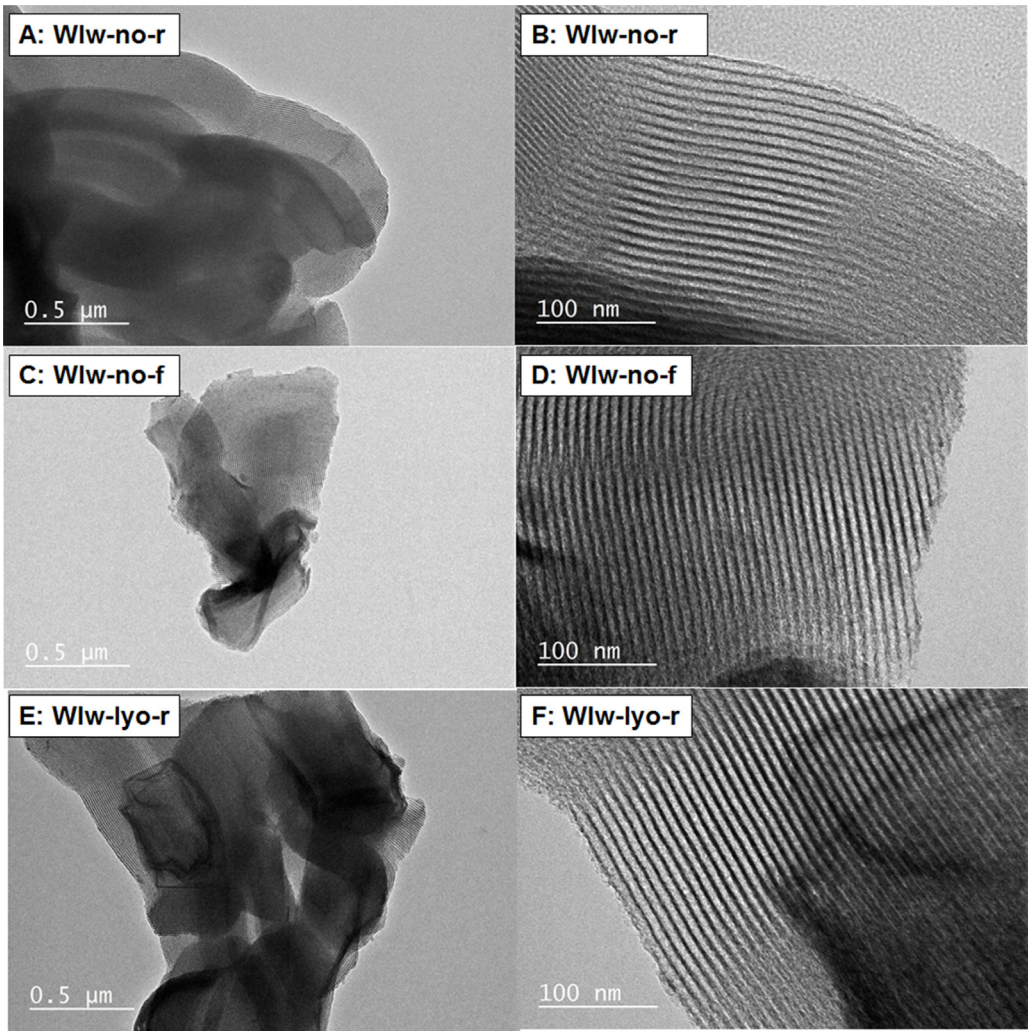

Fig. 8. TEM micrographs of samples WIw-no-r (A and B), WIw-no-f (C and D) and WIw-lyo-r (E and F) obtained by Wet Impregnation in water (WIw).

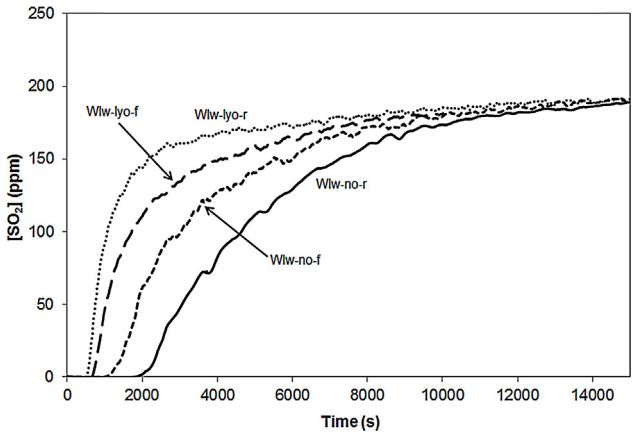

Fig. 9. SO_2 breakthrough curves of samples WIw-no-r, WIw-no-f, WIw-lyo-r and WIw-lyo-f.

Table 3
Synthesis conditions, textural properties, chemical composition and SO_2 uptake capacities of the adsorbents prepared by Incipient Wetness Impregnation with water (IWIw).

Sample	IWIw-45-r	IWIw-90-r	IWIw-lyo-r	IWIw-lyo-f
Drying (24 h)	45 °C	90 °C	Lyoph.	Lyoph.
Calcination	Ramp	Ramp	Ramp	Flash
Color	Green + blue	Dark blue	Blue + green	Green + blue
CuO content (wt. %)	17.3	16.0	15.3	17.6
S_{BET} ($m^2 \cdot g^{-1}$)	532	552	634	518
V_p ($cm^3 \cdot g^{-1}$)	0.7	0.7	0.8	0.7
Pore size (nm)	7.4	7.5	7.7	7.4
SO_2 uptake ($mg_{SO_2} \cdot g_{ads}^{-1}$)	13	4	8	24

accordance with N_2 physisorption isotherms (Fig. 2), the SBA-15 support does not seem to be altered by the impregnation, drying and calcination steps. These results support the bimodal distribution of the copper species; the ratio of large CuO particles to homogeneously dispersed copper species being closely dependent on the drying and calcination conditions.

The SO_2 breakthrough curves of the CuO/SBA-15 samples impregnated in water are shown in Fig. 9.

The highest SO_2 uptake capacities are obtained with adsorbents which were not dried before the calcination step: 49 and 27 $mg_{SO_2} \cdot g_{ads}^{-1}$ for WIw-no-r and WIw-no-f, respectively which accordingly have the smallest XRD diffraction peaks. The lyophilized samples (WIw-lyo-r and WIw-lyo-f) are less efficient (SO_x storage capacities equal to 13 and 18 $mg_{SO_2} \cdot g_{ads}^{-1}$, respectively). As mentioned for the samples impregnated in methanol, it is difficult to correlate the SO_x storage capacity data of these four adsorbents with their corresponding XRD patterns. Indeed, the adsorbent having the highest XRD CuO peaks (sample WIw-no-f) displays a SO_x trapping capacity (27 $mg_{SO_2} \cdot g_{ads}^{-1}$) higher than that of the lyophilized adsorbents (13 and 18 $mg_{SO_2} \cdot g_{ads}^{-1}$) that display nevertheless lower XRD peaks. The efficiency of these adsorbents impregnated with water, is related to the calcination and still more to the drying steps. It seems that the presence of water adsorbed on the material before the calcination step plays a crucial role in regard to the SO_x trapping efficiency. Moreover, the use of water rather than methanol as a solvent seems to favor the formation of efficient copper species for the $DeSO_x$ if one compares the SO_2 uptake capacity data 49 $mg_{SO_2} \cdot g_{ads}^{-1}$ with water; 30 $mg_{SO_2} \cdot g_{ads}^{-1}$ (maximal capacity) with methanol and 15 $mg_{SO_2} \cdot g_{ads}^{-1}$ for the WIm-no-r sample. Here again, the results obtained with water suggest that the $DeSO_x$ efficiency is related to the nature of the XRD-undetected copper species.

3.3. Incipient Wetness Impregnation with water (IWIw)

Since the best performances have been obtained by wet impregnation with water, the IWI was also performed with water. For this series of adsorbents, three drying conditions have been compared (45 °C, 90 °C and lyophilization) with the two calcination methods (ramp and flash). All adsorbents have a copper oxide loading in the range of 15–18 wt. % (Table 3).

As for the sample WIm-90-r obtained by wet impregnation in methanol and dried at 90 °C, the adsorbent IWIw-90-r presents a dark blue color and the XRD pattern exhibits peaks of strong intensity (Fig. 10). This adsorbent is also inefficient for $DeSO_x$. In contrast with the wet impregnation method, the adsorbents calcined with the ramp calcination (IWIw-lyo-r and IWIw-45-r) are heterogeneous in color. Moreover, according to the XRD patterns, it seems that the flash calcination (sample IWIw-lyo-f) limits the formation of large CuO particles (Fig. 10).

The N_2 physisorption isotherms of the IWIw-lyo-r are reported in Fig. 2. It can be seen that the desorption branch is slightly shifted towards higher pressures, an effect usually attributed to cavitation phenomena resulting from pore blocking [37–40]. This phenomenon might be due to the formation of CuO particles in the channels of the SBA-15 structure. Nevertheless, TEM micrographs (Fig. 12) do not evidence the presence of such particles. The pore volumes and BET specific surface areas of the adsorbents prepared by the IWI are similar to those obtained with the wet impregnation method.

The SEM micrographs and the corresponding X-ray mappings of samples IWIw-90-r, IWIw-lyo-r and IWIw-lyo-f are reported in Fig. 11. Similarly to the trend observed above for the sample WIm-90-r, the X-ray mapping of the adsorbent IWIw-90-r (micrograph B) evidences the formation of large CuO particles which is attributed to the drying at "high temperature" (90 °C). The X-ray

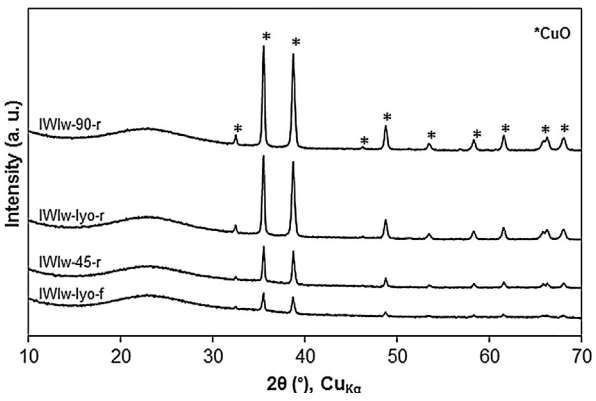

Fig. 10. XRD patterns of CuO/SBA-15 adsorbents prepared by Incipient Wetness Impregnation with water (IWIw). For a better visibility, the diffraction patterns are shifted along the *Y*-axis.

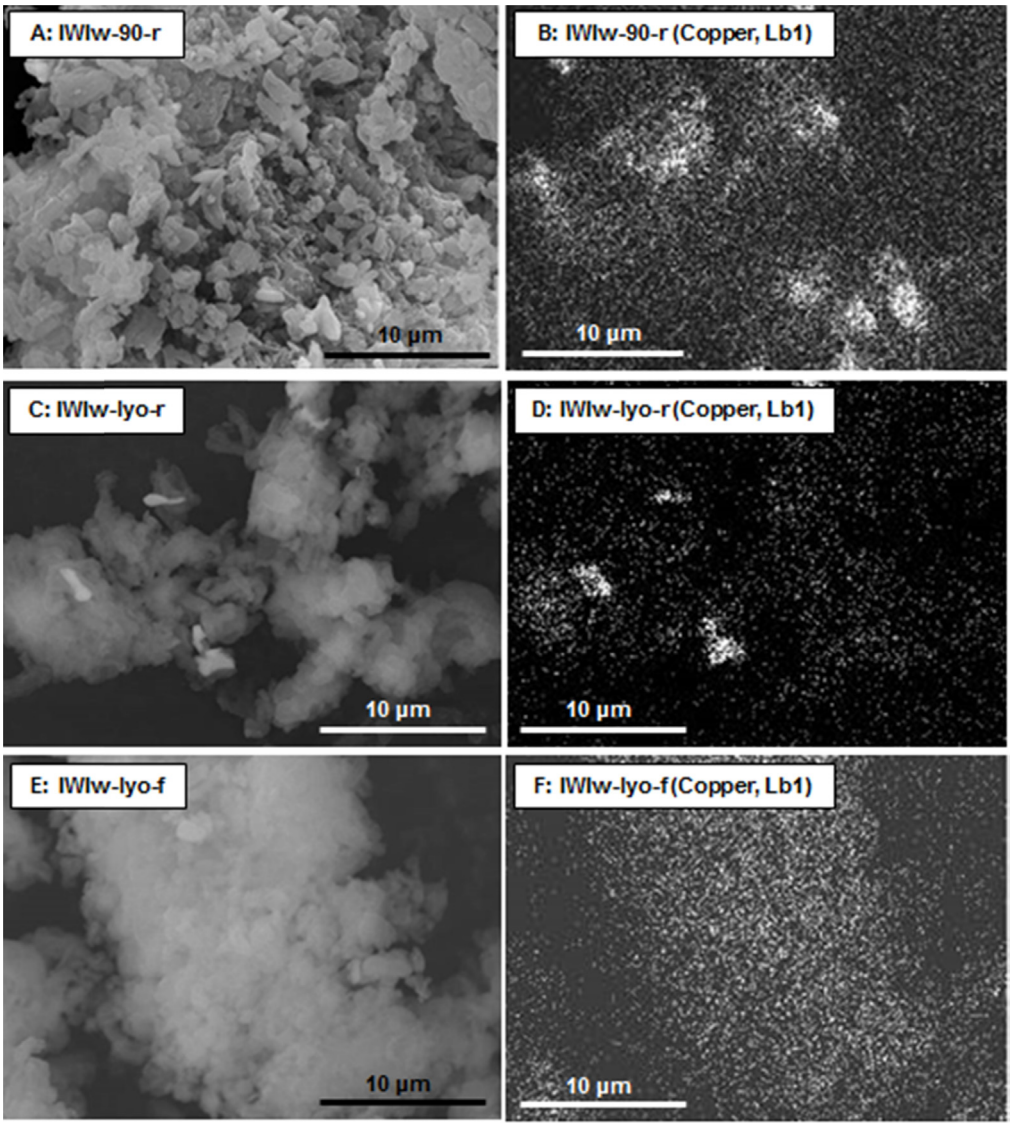

Fig. 11. SEM micrographs (A, C and E) and corresponding X-ray mappings (B, D and F) of samples IWIw-90-r, IWIw-lyo-r and IWIw-lyo-f.

mappings of samples IWIw-lyo-r (Fig. 11D) and IWIw-lyo-f (Fig. 11F) show the formation of large CuO particles in the former while the latter exhibits a homogenous distribution of copper. This result is also in good agreement with the XRD patterns since the IWIw-lyo-r sample exhibits a higher CuO peak intensity (Fig. 10).

Similarly to the preceding results, the TEM micrographs of samples IWIw-lyo-r (A and B) and IWIw-lyo-f (C and D) shown in Fig. 12 confirm that the structure of the mesoporous support is preserved and that no CuO particles are observed, probably due to the formation of Cu–O–Si species or of a thin CuO film.

The SO_2 breakthrough curves of samples IWIw-45-r, IWIw-90-r, IWIw-lyo-r and IWIw-lyo-f are shown in Fig. 13. It is noteworthy that the SO_2 adsorption capacities of the adsorbents prepared by the IWI method are in the same order of magnitude than those of the adsorbents obtained by wet impregnation in methanol. Here also, the sample prepared with a flash calcination leads to the best SO_2 uptake capacity (24 $mg_{SO_2} \cdot g_{ads}^{-1}$) and the one dried at 90 °C the lowest adsorption capacity (4 $mg_{SO_2} \cdot g_{ads}^{-1}$) due to the presence of large CuO particles. For this series of IWI samples, the SO_2 uptake efficiency can be correlated with the XRD patterns since the SO_x adsorption capacity decreases with the increase of the intensity of the XRD peaks of CuO.

3.4. Ion Exchange in water (IEw)

The ion exchange method is well-known to yield well dispersed copper oxide particles due to strong interactions between copper species and the silica support, which prevent the sintering during calcination [41–43]. For this series of adsorbents, four drying conditions were compared

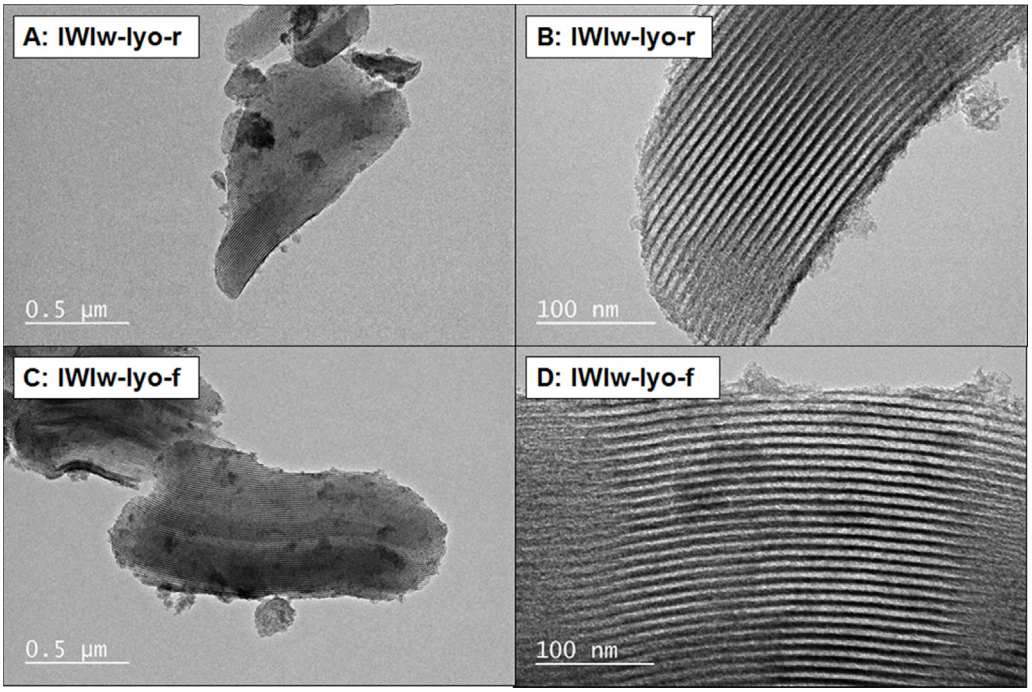

Fig. 12. TEM micrographs of samples IWIw-lyo-r (A and B) and IWIw-lyo-f (C and D) obtained by Incipient Wetness Impregnation in water (IWIw).

(20 °C, 45 °C, 90 °C and lyophilization) and two calcination methods (ramp and flash). The adsorbents had a copper oxide loading in the range of 14–15 wt. % (Table 4), which is smaller than for the previous adsorbents (15–18 wt. %). Contrary to the adsorbents prepared by the other methods, the six adsorbents display the same pale green color, whatever the drying or calcination conditions.

As shown by the XRD patterns of Fig. 14, whatever the drying and calcination conditions, no diffraction peaks of copper oxide are observed, suggesting a strong CuO/SBA-15 interaction. Remarkably, this happens even after a drying at 90 °C.

The N_2 physisorption isotherms of sample IEw-lyo-r reported in Fig. 2 exhibit a stretching of both adsorption and desorption branches in the capillary condensation zone i.e. toward lower pressures (hysteresis loop for P/P^0 from 0.7 to 0.8 for pure SBA-15 versus 0.5 to 0.8 for IEw samples). This suggests that a secondary porosity involving pores smaller than in the starting adsorbent is generated during the ion exchange, which may be due to a partial hydrolysis of silica in the alkaline medium. Probably for the same reason, although the BET specific surface areas (393 to 496 $m^2 \cdot g^{-1}$) are smaller than those reported for the impregnated adsorbents (485 to 637 $m^2 \cdot g^{-1}$), the pore volumes stay in the same order of magnitude (0.7 $cm^3 \cdot g^{-1}$). In spite of the modification of the pore size distribution evidenced by the N_2 isotherms, the pore size remains virtually centered around 7.5 nm.

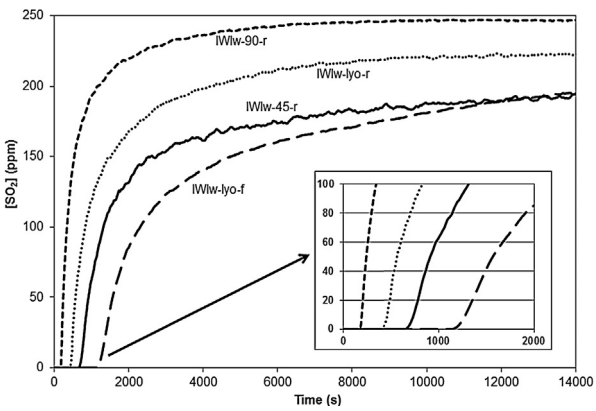

Fig. 13. SO_2 breakthrough curves of samples IWIw-45-r, IWIw-90-r, IWIw-lyo-r and IWIw-lyo-f.

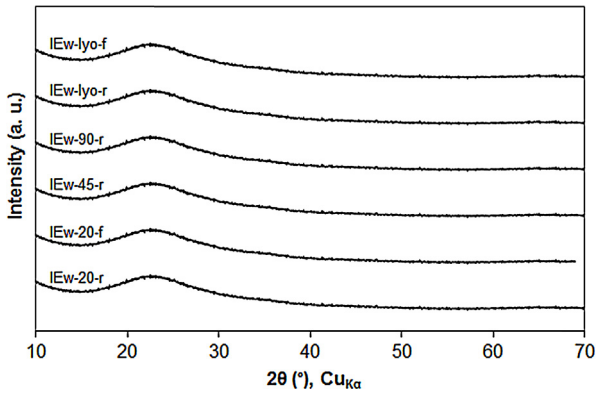

Fig. 14. XRD patterns of CuO/SBA-15 adsorbents prepared by Ion Exchange in water (IEw). For a better visibility, the diffraction patterns are shifted along the Y-axis.

Table 4
Synthesis conditions, textural properties, chemical composition and SO_2 uptake capacities of the adsorbents prepared by Ion Exchange in water (IEw).

Sample	SBA15	IEw-20-r	IEw-20-f	IEw-45-r	IEw-90-r	IEw-lyo-r	IEw-lyo-f
Drying (24 h)	–	20 °C	20 °C	45 °C	90 °C	$T_{amb.}$ + Lyoph.	$T_{amb.}$ + Lyoph.
Calcination	Ramp	Ramp	Flash	Ramp	Ramp	Ramp	Flash
Color	White	Pale green	Pale green	Pale green	Pale green	Pale green	Pale green
CuO content (wt. %)	0	14.7	15.0	15.0	14.4	14.5	14.4
S_{BET} ($m^2 \cdot g^{-1}$)	938	496	485	395	451	452	393
V_p ($cm^3 \cdot g^{-1}$)	1.2	0.7	0.7	0.6	0.7	0.7	0.7
Pore size (nm)	7.5	7.7	7.4	7.6	7.5	7.5	7.5
SO_2 uptake ($mg_{SO_2} \cdot g_{ads}^{-1}$)	/	20	14	13	12	27	22

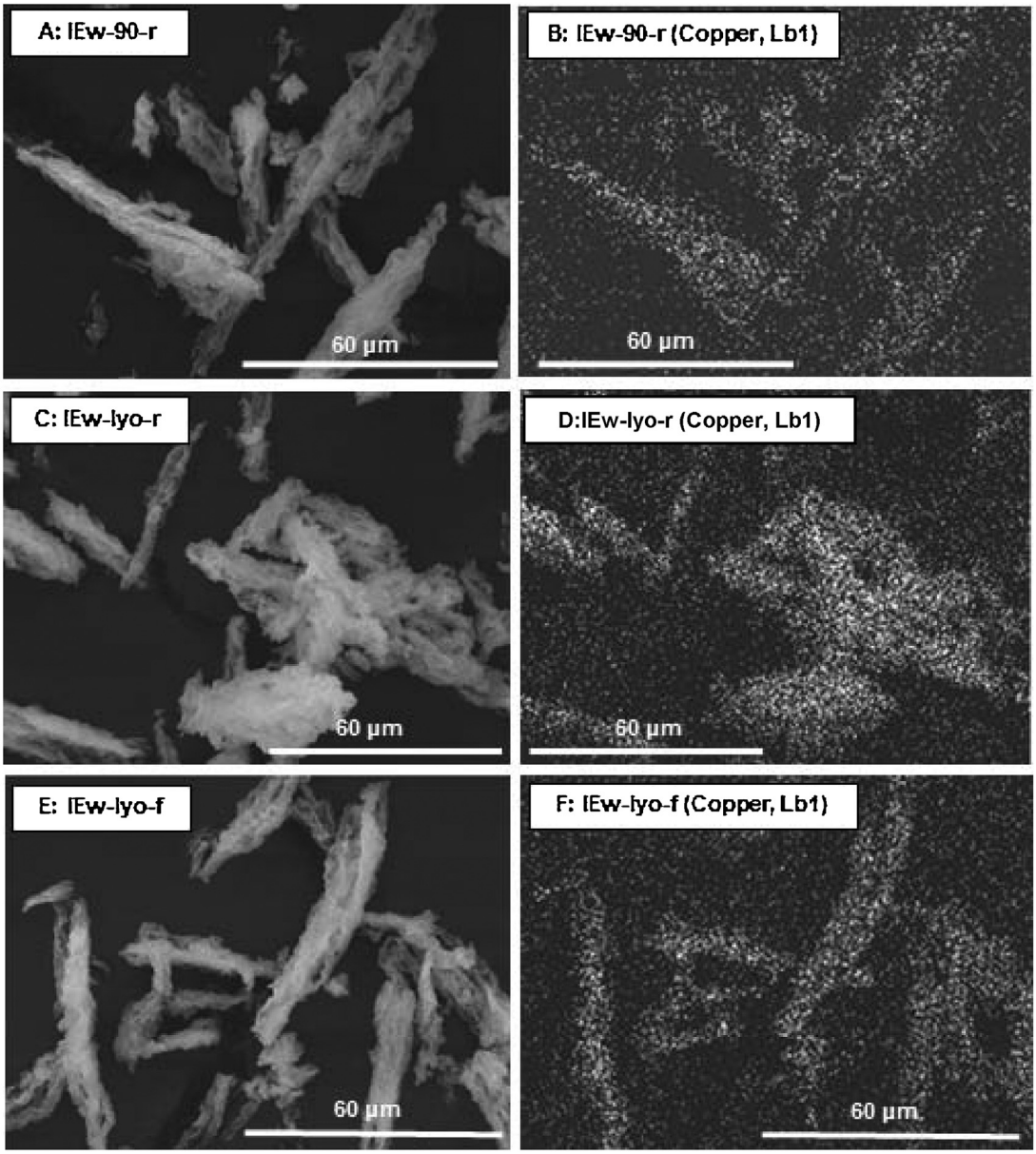

Fig. 15. SEM micrographs (A, C and E) and corresponding X-ray mappings (B, D and F) of samples IEw-90-r, IEw-lyo-r and IEw-lyo-f.

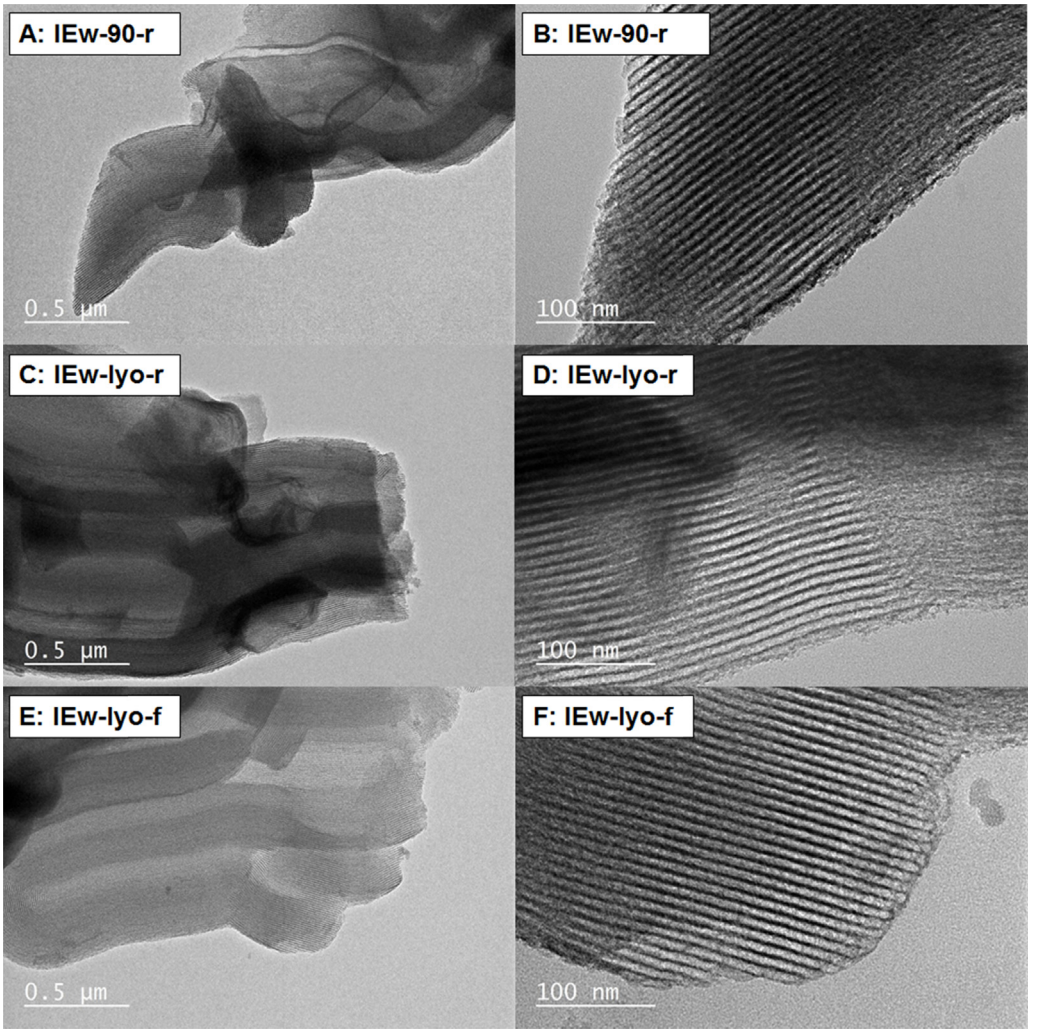

Fig. 16. TEM micrographs of samples IEw-90-r (A and B), IEw-lyo-r (C and D) and IEw-lyo-f (E and F) obtained by Ion Exchange in water (IEw).

The SEM micrographs and the corresponding X-ray mappings (Fig. 15) of the adsorbents IEw-90-r, IEw-lyo-r and IEw-lyo-f confirm that the copper species are homogeneously dispersed regardless of the drying and calcination conditions.

The TEM micrographs (Fig. 16) of samples IEw-90-r (A and B), IEw-lyo-r (C and D) and IEw-lyo-f (E and F) confirm that the structure of SBA-15 is preserved despite the mentioned distortion of the N_2 physisorption pattern. XRD patterns, SEM and TEM micrographs show unambiguously that whatever the drying and calcination conditions, neither large nor small CuO particles are formed with the Ion Exchange method. This can be explained by the strong interaction between the copper species and the support, which prevents particles from coalescing with each other.

The SO_2 breakthrough curves of samples IEw-20-r, IEw-45-r, IEw-90-r and IEw-lyo-r are given in Fig. 17. Like for the other impregnated adsorbents, despite the non-formation of large CuO particles (see XRD patterns), the drying at 90 °C leads to a degradation of the SO_2 adsorption capacity 12 $mg_{SO_2} \cdot g_{ads}^{-1}$. It is also the case after drying at 20 and 45 °C (14 and 13 $mg_{SO_2} \cdot g_{ads}^{-1}$). However, the adsorbent dried at 20 °C (IEw-20-r) exhibits a longer adsorption step, the better result being obtained with the

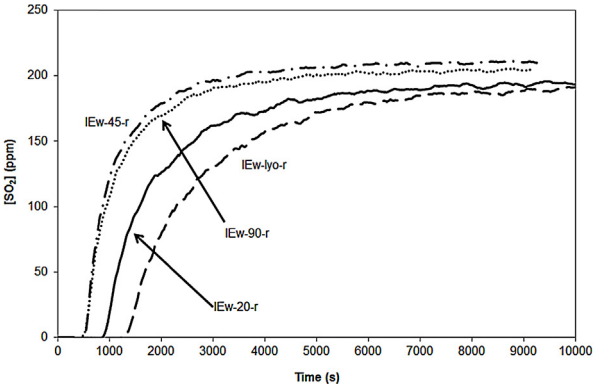

Fig. 17. SO_2 breakthrough curves of samples IEw-20-r, IEw-45-r, IEw-90-r and IE-lyo-r.

lyophilized adsorbent. It seems therefore that, for the samples calcined with a ramp, the decrease of the drying temperature, leads to a better $DeSO_x$ efficiency. The same trend is observed for the adsorbents prepared with the flash calcination although their efficiency remains low.

4. Conclusion

In this work, SBA-15 mesoporous silica was doped with copper oxide by three different methods consisting in wet impregnation, incipient wetness impregnation and ion exchange. The N_2 physisorption data tend to show that the silica support is unaffected by the wet impregnation method, whatever the solvent used (water or methanol). On the contrary, the basic medium (ammonia) used in the ion exchange causes a modification of the porosity resulting in the broadening of the pore size distribution that is assignable to a partial hydrolysis of silica walls. The slight shift towards higher pressures of the N_2 desorption branch that one observes for the incipient wetness impregnated samples is attributed to a partial pore plugging rather than to any alteration of SBA-15 structure. For all impregnated samples series, the interpretation of the XRD patterns suggests a bimodal distribution of copper with the coexistence of:

- a population of large ($\sim$ 1 μm) copper oxide particles;
- a population of homogenously dispersed copper atoms that are XRD-undetectable.

The former population is assumed to come from the coalescence of copper oxide species when the drying step is performed at high temperature, whereby the hydrated copper nitrate molecules tend to concentrate in the wet spots that remain during the last vaporization stages. The latter population is assumed to correspond to a strong copper/support interaction that prevents copper oxide formation from undergoing this coalescence process. As one can expect, it is strongly favored by the ion exchange method, regardless of the drying and calcination conditions. As far as the impregnated samples, the comparison of drying and calcination steps highlights their strong influence on the copper distribution: as a general trend, the drying at low temperature and the use of a calcination ramp, favor the formation of homogenously dispersed copper atoms. On the contrary, the drying at high temperature and the flash calcination entail the formation of large copper oxide particles. The correlation between physicochemical data and $DeSO_x$ experiments is not straightforward. As expected, large CuO particles are poorly efficient, which is attributed to the slow bulk diffusion of the gaseous O_2/SO_2 species. The SO_x trapping efficiency is most probably related to the homogenously dispersed copper atoms. The best result, with a capacity of 49 $mg_{SO_2} \cdot g_{ads}^{-1}$, is obtained by wet impregnation in water, without drying and with ramp calcination. Finally, it must be stressed that the rather modest adsorption performances achieved in this study shall be considered in the light of the high GHSV value that corresponds to a contact time in the range of 0.15 s, a value that has been purposely adopted in this work to specifically address the fast exhaust gas speeds of industrial gas turbines.

Acknowledgment

This work (Project $AdSO_x$ New-Gen – contract #1281C0039) was supported by the French Agency for Environment and Energy Management (ADEME) through its funding program CORTEA. Authors want to acknowledge L. Michelin for XRD characterizations, L. Josien for SEM/EDX analyses and L. Vidal for TEM characterizations.

References

[1] A.P. Tsimpidi, V.A. Karydis, S.N. Pandis, J. Air Waste Manage. 57 (12) (2007) 1489.
[2] Y. Mathieu, L. Tzanis, M. Soulard, J. Patarin, M. Vierling, M. Moliere, Fuel Process. Technol. 114 (2013) 81.
[3] G. Centi, N. Passarini, S. Perathoner, A. Riva, Ind. Eng. Chem. Res. 31 (1992) 1947.
[4] R. McCabe, W. Chun, G. Graham, C. Montreuil, B, Carberry, A. Chigapov, A. Dubkov, 2005 patent US 2005/0145827.
[5] S.S. Pollack, W.P. Chisholm, R.T. Obermyer, S.W. Hedges, M. Ramanathan, P.A. Montano, Ind. Eng. Chem. Res. 27 (1988) 2276.
[6] K.S. Yoo, S.D. Kim, S.B. Park, Ind. Eng. Chem. Res. 33 (1994) 1786.
[7] X. Zhong, J. Barbier Jr., D. Duprez, H. Zhang, S. Royer, Appl. Catal., B – Environ. 121–122 (2012) 123.
[8] A. Ungureanu, B. Dragoi, A. Chirieac, S. Royer, D. Duprez, E. Dumitriu, J. Mater. Chem. 21 (2011) 12529.
[9] L.-F. Chen, P.-J. Guo, L.-J. Zhu, M.-H. Qiao, W. Shen, H.-L. Xu, K.-N. Fan, Appl. Catal., A – Gen. 356 (2009) 129.
[10] X. Guo, A. Yin, W.-L. Dai, K. Fan, Catal. Lett. 132 (2009) 22.
[11] N. Brodie-Linder, R. Besse, F. Audonnet, S. LeCaer, J. Deschamps, M. Impéror-Clerc, C. Alba-Simionesco, Micropor. Mesopor. Mat. 132 (2010) 518.
[12] Y.M. Wang, Z.Y. Wu, J.H. Zhu, J. Solid State Chem. 177 (2004) 3815.
[13] M. Imperor-Clerc, D. Bazin, M.D. Appay, P. Beaunier, A. Davidson, Chem. Mater. 16 (2004) 1813.
[14] I. Lopes, N. El Hassan, H. Guerba, G. Wallez, A. Davidson, Chem. Mater. 18 (2006) 5826.
[15] M.N. Kaydouh, N. El Hassan, A. Davidson, S. Casale, H. El Zakhem, P. Massiani, C.R. Chim. 18 (2015) 293.
[16] L. Vradman, M.V. Landau, D. Kantorovich, Y. Koltypin, A. Gedanken, Micropor, Micropor. Mesopor. Mat. 79 (2005) 307.
[17] S.L. Soled, E. Iglesia, R.A. Fiato, J.E. Baumgartner, H. Vroman, S. Miseo, Top. Catal. 26 (2003) 101.
[18] T. Toupance, M. Kermarec, C. Louis, J. Phys. Chem. B 104 (2000) 965.
[19] P. Mäki-Arvela, D.Y. Murzin, Appl. Catal., A – Gen. 451 (2013) 251.
[20] F. Négrier, E. Marceau, M. Che, J.-M. Giraudon, L. Gengembre, A. Löfberg, J. Phys. Chem. B 109 (2005) 2836.
[21] S.-S. Lee, H.-I. Park, B.-K. Park, S.-H. Byeon, Mat. Sci. Eng. B – Solid 135 (2006) 20.
[22] M. Che, Z.X. Cheng, C. Louis, J. Am. Chem. Soc. 117 (1995) 2008.
[23] J.R.A. Sietsma, J.D. Meeldijk, J.P. den Breejen, M. Versluijs-Helder, A. Jos van Dillen, P.E. de Jongh, K.P. de Jong, Angew. Chem. Int. Ed. 46 (2007) 4547.
[24] J. van de Loosdrecht, S. Barradas, E.A. Caricato, N.G. Ngwenya, P.S. Nkwanyana, M.A.S. Rawat, B.H. Sigwebela, P.J. van Berge, J.L. Visagie, Top. Catal. 26 (2003) 121.
[25] P. Munnik, M. Wolters, A. Gabrielsson, S.D. Pollington, G. Headdock, J.H. Bitter, P.E. de Jongh, K.P. de Jong, J. Phys. Chem. C 115 (2011) 14698.
[26] J.R.A. Sietsma, H. Friedrich, A. Broersma, M. Versluijs-Helder, A.J. van Dillen, P.E. de Jongh, K.P. de Jong, J. Catal. 260 (2008) 227.
[27] K. P. De Jong, P.E. De Jongh, J.R. A. Sietsma, A.J. Van Dillen, 2009. [Patent EP2061595].
[28] A. Hahn, T. Ressler, R.E. Jentoft, F.C. Jentoft, Chem. Commun. (2001) 537.
[29] J.R.A. Sietsma, J.D. Meeldijk, M. Versluijs-Helder, A. Broersma, A.J. van Dillen, P.E. de Jongh, K.P. de Jong, Chem. Mater. 20 (2008) 921.
[30] B. Vos, E. Poels, A. Bliek, J. Catal. 198 (2001) 77.
[31] M. Wolters, L.J.W. van Grotel, T.M. Eggenhuisen, J.R.A. Sietsma, K.P. de Jong, P.E. de Jongh, Catal. Today 163 (2011) 27.
[32] X. Sun, Y. Shi, P. Zhang, C. Zheng, X. Zheng, F. Zhang, Y. Zhang, N. Guan, D. Zhao, G.D. Stucky, J. Am. Chem. Soc. 133 (2011) 14542.
[33] A.H. Janssen, C.-M. Yang, Y. Wang, F. Schüth, A.J. Koster, K.P. de Jong, J. Phys. Chem. B 107 (2003) 10552.

[34] W.-H. Tian, L.-B. Sun, X.-L. Song, X.-Q. Liu, Y. Yin, G.-S. He, Langmuir 26 (2010) 17398.
[35] X.C. Shao, L.-H. Duan, Y.-Y. Wu, Y.-C. Qin, W.-G. Yu, Y. Wang, H.-L. Li, Z.-L. Sun, L.-J. Song, Acta Phys. Chim. Sin. 28 (2012) 1467.
[36] F. Rouquerol, J. Rouquerol, K. Sing, Adsorption by powders and porous solids: principles, methodology and applications, Academic Press (Elsevier), 1999.
[37] P. Van Der Voort, P.I. Ravikovitch, K.P. De Jong, M. Benjelloun, E. Van Bavel, A.H. Janssen, A.V. Neimark, B.M. Weckhuysen, E.F. Vansant, J. Phys. Chem. B 106 (2002) 5873.
[38] A.V. Neimark, P.I. Ravikovitch, A. Vishnyakov, Phys. Rev. E 62 (2000) R1493.
[39] A.Y. Khodakov, V.L. Zholobenko, R. Bechara, D. Durand, Micropor. Mesopor. Mat. 79 (2005) 29.
[40] P.I. Ravikovitch, A.V. Neimark, J. Phys. Chem. B 105 (2001) 6817.
[41] M.A. Kohler, J.C. Lee, D.L. Trimm, N.W. Cant, M.S. Wainwright, Appl. Catal. 31 (1987) 309.
[42] L. Jiao, J.R. Regalbuto, J. Catal. 260 (2008) 329.
[43] L. Jiao, J.R. Regalbuto, J. Catal. 260 (2008) 342.